Extremum Seeking Control of Tunable Thermoacoustic Cooler*

Yaoyu Li†, Mario A. Rotea‡, George T.-C. Chiu†, Luc G. Mongeau†, In-Su Paek†

Abstract— **The performance of a prototype standing wave thermoacoustic cooler is optimized using an extremum seeking control algorithm. A tunable Helmholtz resonator was developed for a thermoacoustic cooler to change the boundary condition of the standing wave tube. The volume of the resonator is adjusted by changing the location of a piston on a ball-screw assembly driven by a DC motor. Multi-parameter extremum seeking control (ESC) was applied to optimize the cooling power via tuning of both the boundary condition (piston location) and the driving frequency. Experiments were conducted under both fixed and varying operating conditions. The experimental results demonstrated the effectiveness of ESC.**

Index Terms — **Thermoacoustic cooler, tunable Helmholtz resonator, extremum seeking control.**

I. Introduction

OVER the past twenty years, extensive research efforts have been made to develop thermoacoustic heat pumping systems that use high amplitude sound waves in acoustically sealed vessels to realize refrigeration [1] [2]. Such systems do not require phase-change refrigerants and use inert gases as their working fluids, which is an environmentally benign alternative.

Figure 1 shows the schematic of a half wavelength standing wave thermoacoustic cooler driven by an electro-dynamic driver. The standing wave tube contains pressurized inert gas as the working medium. The hot and cold heat exchangers along with properly designed stacks are installed close to the driver, where the pressure amplitude is relatively large and the velocity amplitude is relatively small. Along the stack plates, due to standing acoustic waves, the gas parcels experience periodic compression and expansion. During the first half cycle, the gas parcels are expanded as they move towards the cold side. If the gas temperature decreases to lower than that of the neighboring stack surface, heat is absorbed from the stack surface to the gas. During the second half cycle, the gas parcels are compressed and moved towards the hot side. If the gas temperature is higher than that of the neighboring stack surface, heat is released to the stack surface. A Brayton refrigeration cycle is thus completed. Since many such cycles run in concatenation on the stack surface along the longitudinal direction, a temperature gradient is formed. With heat exchangers installed at both ends of the stack and connected to the exterior sources, a cooling system is obtained.

For a thermoacoustic refrigerator driven by an electrodynamic driver, the actual physical process is complex due to the coupled electroacoustic, thermodynamic and fluid mechanical processes. The energy flow can be separated into two stages. The first stage is to convert electrical energy into acoustic energy, and the second stage is to utilize acoustic energy in heat pumping. The overall efficiency for the system is determined by the combined performance of the two stages. Optimizing the performance of the first stage has been considered as a purely acoustic problem. Nominal design is conducted with existing thermoacoustic modeling packages. Driver parameters are selected to match the nominal operating conditions. Manual tuning of driver parameters such as spring stiffness is also required to compensate for the inaccuracies in modeling the actual system. This procedure is tedious and expensive. Moreover, a fixed setup cannot deal with the time-varying behavior for such devices. A tunable system is necessary to maintain good performance.

Reference [3] investigated the on-line tuning of the driving frequency for maximizing the acoustic efficiency. It showed that feedback control using measurements like sound pressure, piston velocity, coil voltage or current cannot affect the driver efficiency. The driver efficiency can only be affected by driver parameters, acoustic duct dimensions, gas mixture, cooling load and driving frequency. The experimental results showed that it is feasible to search for maximum achievable acoustic efficiency by tuning the driving frequency on line. However, tuning the driving frequency alone is not sufficient to maintain

* This work was supported in part by NSF Award 0080832-ECS
† Ray W. Herrick Laboratories, School of Mechanical Engineering, Purdue University, West Lafayette, IN 47907-2031, USA.
‡ School of Aeronautics and Astronautics, Purdue University, West Lafayette, IN 47907-2023, USA. (corresponding author; phone: 765-494-6212; fax: 765-494-0307; e-mail: rotea@purdue.edu).

the best achievable performance for a given set of driver parameters. In theory, there exists an optimally matched acoustic impedance for a given driver to obtain the highest possible acoustic performance, which may be approximated by tuning the boundary condition. The combination of driving frequency and boundary condition tuning, provides a vehicle for performance optimization of a thermoacoustic cooler.

Boundary condition tuning can be obtained using a tunable Helmholtz resonator as in noise control applications [4] [5]. Early tunable resonators were manually tuned [4]. Automated tunable resonators were developed in the 1990s [5]. The complex nature of the thermoacoustic process has limited the development of efficient tuning algorithms. Recent advancements in extremum seeking control (ESC) [6] [7] have provided analytical results and guidelines for stable tuning algorithms with rapid convergence without requiring detailed plant information. In the present paper, multi-parameter ESC is employed to tune the length of a Helmholtz resonator and the driving frequency to attain and track the optimal cooling power despite changes in operating condition.

II. TUNABLE HELMHOLTZ RESONATOR FOR THERMOACOUSTIC COOLER

The schematic of the tunable Helmholtz resonator system is shown in Fig. 2. The thermoacoustic cooler is driven by a 300 Watt moving-magnet electro-dynamic driver, with the heat exchangers and the circular stack installed close to the driver. The 15 cm-diameter resonator is attached to the cold adapter via a streamlined connector (see [8] for design details). A DC motor drives a piston via a ball-screw assembly to change the resonator volume, and thus the system impedance. The piston position was measured by the encoder mounted to one end of the motor shaft. The static pressures on both sides of the piston are balanced by connecting both sides of the piston with a 0.95 cm-diameter stainless-steel tube. The high acoustic impedance of the hose acts as a low pass acoustic filter that balances the DC pressure between the two chambers but isolates the higher frequency acoustic signals. A pressure sensor and an accelerometer are used to measure the sound pressure and the piston velocity of the driver, respectively. The driver coil voltage and current are measured using a voltage divider and an HP-1146A current probe, respectively. Thermocouples and mass flow sensors are installed at the heat exchangers to measure temperatures and flow rates.

III. EXTREMUM SEEKING CONTROL

It is difficult to optimize the cooling performance of the device without some form of experiment-based tuning. This section describes the extremum seeking control (ESC) algorithm used to optimize cooling performance by adjusting the driving frequency and piston position.

Research in ESC was popular in the 1950s and 1960's [9]. A resurgence in this area was ignited in recent years. Krstić and Wang provided a stability proof for general SISO nonlinear plant using averaging and singular perturbation methods [6]. Multi-parameter tuning was studied later by Rotea [7] who gave design guidelines for ESC. Later, Ariyur and Krstić [10] considered multi-parameter ESC for problems where the optimal parameters have partially known variations with time. The design procedures proposed in [7] and [10] are similar in many aspects. The framework in [7] is used in this paper.

ESC considers the problem of finding an optimizing input $u_{opt}(t)$ for the generally unknown time-varying cost function $l(t,u)$:

$$u_{opt}(t) = \arg\min_{u \in \mathbb{R}^m} l(t,u), \qquad (1)$$

where $u(t) \in \mathbb{R}^m$ is the input parameter vector. Figure 3 shows the block diagram for a typical ESC system. The measurement of the cost function $l(t,u)$ is corrupted by noise $n(t)$ and it is denoted by $y(t)$. The transfer function $F_I(s)$ denotes the linear dynamics of the mechanism that commands the parameter vector $u(t)$. $F_O(s)$ denotes the transfer function of the sensor dynamics that measures the cost function, which is often a low-pass filter for removing noise. The basic components in a typical ESC system are $d_1^T(t)=\left[\sin(\omega_1 t) \ \cdots \ \sin(\omega_m t)\right]$ and $d_2^T(t) = \left[a_1 \sin(\omega_1 t + \alpha_1) \ \cdots \ a_m \sin(\omega_m t + \alpha_m)\right]$, the perturbation or dither signals, which in conjunction with the high-pass filter $F_{HP}(s)$ and the low-pass filter $F_{LP}(s)$, produce a signal proportional to the gradient $\frac{\partial l}{\partial u}(\hat{u})$.

To achieve local optimality for the optimization problem in Eq. (1), it is desirable to drive this gradient vector to zero. Integrating the output signal of the low pass filter $F_{LP}(s)$ would achieve this purpose asymptotically. Adding a suitable dynamic compensator $K(s)$ may improve the transient performance of the extremum seeking. Further details may be found in [7].

In the rest of this section, the low-pass filter $F_{LP}(s)$ and the input dynamics $F_I(s)$ in Fig. 3 are assumed diagonal. Since the output dynamics of the tunable thermoacoustic cooler can be neglected, we assume that $F_O(s) = 1$. The tunable device has two adjustable parameters, the piston position and the driving frequency; hence, the length of the input vector u is $m = 2$.

To have a working ESC algorithm the following parameters need to be designed: dither amplitudes $a_1,\ldots, a_m$; dither frequencies $\omega_1, \ldots, \omega_m$; dither phase angles $\alpha_1, \ldots, \alpha_m$; low-pass filter $F_{LP}(s)$; high-pass filter $F_{HP}(s)$; and the dynamic compensator $K(s)$. Rotea [7] provided the following guidelines for designing these parameters.

Basic guidelines. The dither frequencies ω_1 and ω_2 should be distinct. These frequencies must be in the pass-band of the high-pass filter $F_{HP}(s)$ and in the stop-band of the low-pass filter $F_{LP}(s)$. The dither frequencies should be high but should not excite unmodeled plant dynamics; preferably, these frequencies should below the first corner frequency of $F_1(s)$.

Guidelines to improve steady-state tracking of optimal parameters. The dither phase angles α_1 and α_2 should satisfy $-\frac{\pi}{2}<\angle F_{1,i}(j\omega_i)+\alpha_i<\frac{\pi}{2}$, where $F_{1,i}(s)$ denotes the i-th diagonal entry of $F_1(s)$. The closer the angle

$$\theta_i = \angle F_{1,i}(j\omega_i) + \alpha_i \tag{2}$$

is to zero, the better the steady-state accuracy.

Guidelines for stability and transient convergence properties. The linear (small signal) stability properties of the ESC in Fig. 3 may be determined from the characteristic equation

$$\det\left[I - G(s)RQ\right] = 0 \tag{3}$$

where $G(s)$ is given by

$$G(s) = -\frac{F_1(s)K(s)F_{LP}(s)}{s} \tag{4}$$

while the matrix R is defined to be

$$R = \frac{1}{2}\begin{pmatrix} a_1\left|F_{1,1}\left(j\omega_1\right)\right|\cos\left(\theta_1\right) & 0 \\ 0 & a_2\left|F_{1,2}\left(j\omega_2\right)\right|\cos\left(\theta_2\right) \end{pmatrix} \tag{5}$$

with θ_1 and θ_2 given by Eq. (2). The matrix Q in the characteristic Eq. (3) is the Hessian of the cost function at the optimal solution of the problem in Eq. (1). That is, Q is a symmetric matrix satisfying

$$l(t,u) \approx u_{opt} + \frac{1}{2}\left(u-u_{opt}\right)^T Q\left(u-u_{opt}\right) \tag{6}$$

when u is sufficiently close to u_{opt}.

IV. EXPERIMENTAL RESULTS

The control goal is to *maximize the cooling power*, which is defined as

$$\dot{Q}_c = C_p \dot{m}_c \Delta T_c \tag{7}$$

where C_p is the specific heat at constant pressure, $\dot{m}_c$ is the measured mass flow rate of the water flowing through the cold-side heat exchanger, and ΔT_c is the temperature gradient across the heat exchanger measured by the thermopile.

The input dynamics $F_1(s)$ from frequency and position tuning to cooling power was estimated with several step responses under different input levels [8]. The step responses of the system indicated first-order behavior for both tuning channels. The following first-order models were used to fit the step response data [8]:

$$F_{1f}(s) = \frac{1}{T_{1f}s+1} \quad \text{and} \quad F_{1x}(s) = \frac{1}{T_{1x}s+1}, \tag{8}$$

with T_{1f} set at 4 second and T_{1x} at 6 second.

The fundamental period of the dither signals is set at 10 times the time constant of its input dynamics. That is

$$\omega_f = \frac{2\pi}{10T_{1f}} = 0.157 \text{ rad/s}, \ \omega_x = \frac{2\pi}{10T_{1x}} = 0.105 \text{ rad/s} \tag{9}$$

The next step is to choose the high-pass filter $F_{HP}(s)$. The magnitude response of $F_{HP}(s)$ should be close to one at the smaller of the two dithering frequencies. The following high-pass filter was selected:

$$F_{HP}(s) = \frac{s^2}{s^2 + 0.0928s + 0.0064}, \tag{10}$$

which has a unity gain at ω_x. The low-pass filters are designed to be identical and to attenuate the smaller dither frequency ω_x. The low pass filter was selected as:

$$F_{LP}(s) = \frac{0.0036}{s^2 + 0.072s + 0.0036}, \tag{11}$$

which has magnitude attenuation in excess of 9dB at ω_x.

The dither signals are $d_1^T(t) = \left[\sin\left(\omega_x t\right) \ \sin\left(\omega_f t\right)\right]$ and $d_2^T(t) = \left[a_x \sin\left(\omega_x t + \alpha_x\right) \ a_f \sin\left(\omega_f t + \alpha_f\right)\right]$, where a_x and a_f are dithering magnitude for position and frequency tuning, respectively. From the guideline for improved tracking, the appropriate angles are $\alpha_f = \alpha_x = 0.18\pi$ (rad), which results in $\theta_f = \theta_x = 0.26°$. The dithering amplitudes were selected as $a_x = 0.25$ cm and $a_f = 0.2$ Hz.

The experiments were conducted under several different scenarios: (1) extremum seeking with fixed operating condition; (2) extremum seeking with varying operating condition, specifically, a step change of cold-water flow rate, and (3) comparison of transient performance with different compensator $K(s)$ design.

The operating condition in this context includes the parameters that may change during continuous operation such as the flow rates, the inlet temperatures, the mean pressure of the resonator, the gas constituents, the ambient air temperature and the input voltage to the power amplifier. All these factors may change the performance of the thermoacoustic cooler.

A diagonal PD controller was chosen as the basic form for the compensator $K(s)$ in Fig. 3, i.e.

$$K(s) = \begin{bmatrix} K_{px} + K_{dx}s & 0 \\ 0 & K_{pf} + K_{df}s \end{bmatrix} \quad (12)$$

in which subscript x and f indicate the piston position and the frequency tuning channel, respectively. This form of dynamic compensator was shown to stabilize a Simulink simulation of the entire system [8], in which the static mapping from the piston position x and the driver frequency f to the cooling power $\dot{Q}_c$ was approximated with the experimental data as shown in Table 1.

The ESC algorithm was implemented on an Agilent E8403A VXI mainframe. Three E1432 acoustic boards were used for acquiring the acoustic, electric, position, flow and thermal measurements and for sending out the command signals for the loudspeaker and the piston position. Temperature and flow rate measurements were used to calculate the cooling power according to Eq. (7).

A. Fixed Operating Condition

The system was started at a non-optimal piston position and driving frequency, and the controller was turned on to bring the system to the optimum. From the open-loop static measurements in Table 1, the maximum cooling power can be achieved when the piston is between 15 and 17.5 cm, and the driving frequency between 147 and 149 Hz. The maximum cooling power at this condition is about 41.3 Watt.

The test was conducted with the piston starting at 10 cm and the driving frequency at 141 Hz. A proportional controller was used for $K(s)$ with $K_{px} = 6$, $K_{pf} = 8$. Figure 4 shows the time histories of the measured cooling power, piston position and driving frequency. The ESC was turned on at about 40 seconds, and it brought the system to a new steady state operating condition with the piston position and driving frequency at 15.9 cm and 146.7 Hz, respectively, achieving the cooling power of 42.5 Watt. The achieved steady state (cooling power, piston and driving frequency) is very close to the optimum shown in Table 1.

B. Varying Operating Condition

To evaluate the performance of the ESC in tracking varying operating conditions, a step change was introduced to the cold-side flow rate, which changed the cooling load. The controller $K(s)$ used was the proportional controller of the previous test. As shown in Fig. 5, the flow rates started with 34 and 33 ml/sec. The cold-side flow rate was suddenly increased from 34 to 69 ml/sec at 153 second. The initial position and frequency were set at 15.2 cm and 142 Hz, respectively. The controller was turned on for about 2 minutes before increasing the flow rate to ensure that the steady state associated with the initial flow rates was reached. For the initial flow rate setting, the optimal steady-state cooling power was 51.5 Watt, with piston position and driving frequency at 23.3 cm and 153.4 Hz, respectively. For the new flow rate, after the perturbation at 153 second, the steady-state cooling power was 57.6 Watt with 12.8 cm and 144.9 Hz. It took about 80 seconds for the input parameters to settle to their optimal steady-state values.

C. Comparison of Different Compensators

As indicated in [7] and [10], using PD compensator may improve the transient performance of extremum seeking. Both P-control and PD-control were used to compare the transient performance. The starting input parameters were set at 15 cm and 142 Hz for all cases. The mean pressure, the flow rates and inlet temperatures were maintained constant during the tests. The dithering amplitudes for both channels were kept same as those in the previous two tests.

Figure 6 shows the results for Test *A*, where P-controller was used for $K(s)$, with $K_{px} = 4$ and $K_{pf} = 6$. Figure 7 shows the results of Test *B*, where relatively small derivative gains were used. Figure 8 shows the results of Test *C*, where larger derivative gains were used. Figure 9 showed the results of Test *D*, where the system became unstable under very large derivative gains.

Comparing the experimental results from Test *A* and Tests *B* and *C*, it is clear that adding the derivative term reduces the settling time, and thus improves the transient performance. Adding excessive derivative action tends to increase oscillation amplitudes for the steady state response. This is observed by comparing the results of Test *B* and Test *C*. For Test *C*, the cooling power showed significantly more oscillation due to larger derivative action. Finally, Test *D* showed even larger derivative action destabilized the system. Table 2 summarizes the controller parameters and results of the comparison tests.

D. Remarks

It is noteworthy that the achievable optimal cooling power and its corresponding input parameters vary from test to test, see Figs. 4 through 9. This is due to the variation of the spring plate characteristics. During the testing, the plate became softer and softer and finally failed. Thus the system characteristics kept changing throughout the testing process. These variations are real and, thus, they indicated the need for a tunable device that can adjust the input parameters to attain the maximum achievable performance under varying system characteristics.

V. CONCLUSIONS AND DISCUSSION

An ESC algorithm was proposed and implemented for optimizing the performance of a thermoacoustic cooler. A tunable Helmholtz resonator was developed. Multi-parameter ESC was applied to maximize the cooling power. Experiments were conducted to search for the optimal cooling power with fixed and varying operating conditions. The experimental results showed the effectiveness of using ESC for tuning the resonator to optimize the performance of a thermoacoustic cooler.

REFERENCES

[1] G. W. Swift, "Thermoacoustic engines". *J. Acoust. Soc. Am.*, **84** (4), 1145-1180. October, 1988.

[2] S. L. Garrett and S. Backhaus, "The Power of Sound". *American Scientist*. Volume 88, No. 6, 516-525. November-December 2000.

[3] Y. Li, B. L. Minner, G. T.-C. Chiu, L. G. Mongeau and J. E. Braun, **"**Adaptive Tuning of an Electro-Dynamically Driven Thermoacoustic Cooler". *J. Acoust. Soc. Am.*, **111 (3)**, 1251-1258, March 2002.

[4] Koopman G. and Neise W. "Reduction of centrifugal fan noise by use of resonators". *J. Sound Vib.*, 73, 297-308. 1980.

[5] de Bedout, J M. Franchek, M A. Bernhard, R J. Mongeau, L. "Adaptive-passive noise control with self-tuning Helmholtz resonators". *J. Sound Vib.*. Vol. 202, No. 1, 109-123. April, 1997.

[6] M. Krstić and H.-H. Wang, "Stability of Extremum Seeking Feedback for General Nonlinear Dynamic Systems". *Automatica* **36**, 595-601. 2000.

[7] M. A. Rotea, "Analysis of Multivariable Extremum Seeking Algorithm". *Proceedings of American Control Conference*, 433- 437. Chicago, IL. June 2000.

[8] Y. Li, M. A. Rotea, G. T.-C. Chiu, L. G. Mongeau and I.-S. Paek, "Extremum seeking control for tunable thermoacoustic coolers", submitted to *IEEE Transactions on Control System Technology*.

[9] P. F. Blackman, "Extremum–Seeking Regulators". *An Exposition of Adaptive Control*. Pergamon Press. 1962.

[10] K. B. Ariyur and M. Krstić, "Analysis and Design of Multivariable Extremum Seeking". *Proceedings of American Control Conference*, 2903-2908. Anchorage, AK. May 2002.

Table 1: Static map from the piston position and driving frequency to the cooling power at 2 MPa mean pressure

Piston Position x (cm)	Driving Freq. f (Hz)	Cooling Power $\dot{Q}_c$ (W)	
10	141	22.65	
10	142	29.92	
10	143	35.67	
10	144	28.63	
10	145	21.25	
12.5	142	15.89	
12.5	144	34.12	
12.5	145	39.68	
12.5	146	35.12	
12.5	148	19.34	
15	140	4.95	
15	142	9.00	
15	144	18.55	
15	145	23.86	
15	146	35.99	optimum
15	**147**	**41.28**	←
15	148	38.00	
15	149	30.36	
15	150	19.36	
17.5	146	16.34	
17.5	148	33.34	
17.5	149	41.21	
17.5	150	40.70	
17.5	151	34.69	
17.5	153	19.63	
20	151	32.16	
20	152	35.60	
20	153	31.74	

Table 2: Summary of the comparison tests

Test No.	*A*	*B*	*C*	*D*
K_{px}	4	4	4	4
K_{dx}	0	2	4	20
K_{pf}	6	6	6	6
K_{df}	0	3	6	20
Steady-state cooling power (W)	54.47	60.63	58.2	N/A
5% Settling time (sec.)	109	58	56	N/A
Steady-state position (cm)	21.3	25.3	26.5	N/A
Steady-state driving freq. (Hz)	152.3	156	157.2	N/A

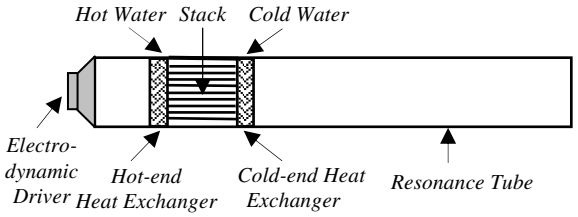

Fig. 1: Schematic of a standing wave thermoacoustic cooler

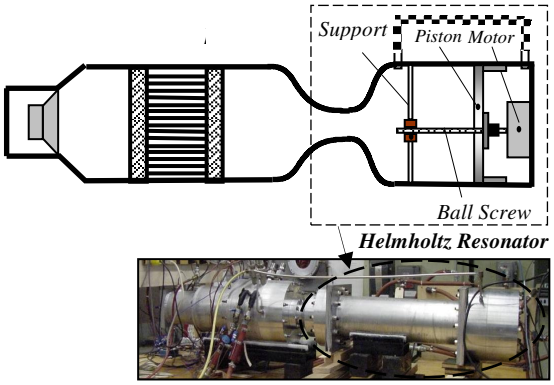

Fig. 2: Schematic of the thermoacoustic cooler with tunable Helmholtz resonator

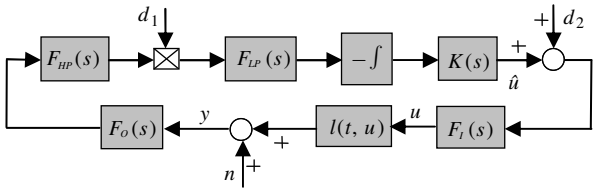

Fig. 3: Block diagram of ESC algorithm

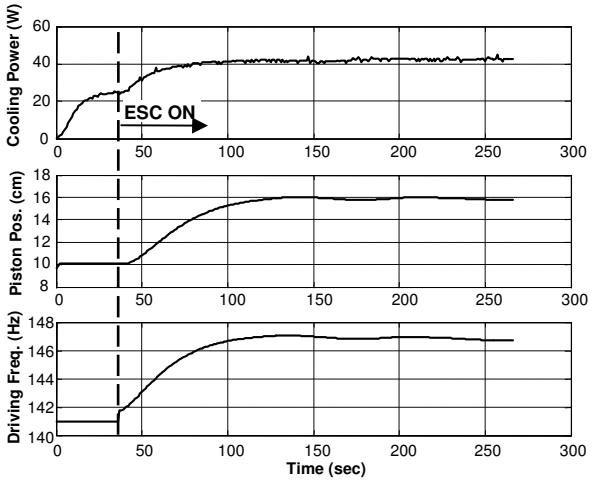

Fig. 4: ESC Tuning with fixed operating condition

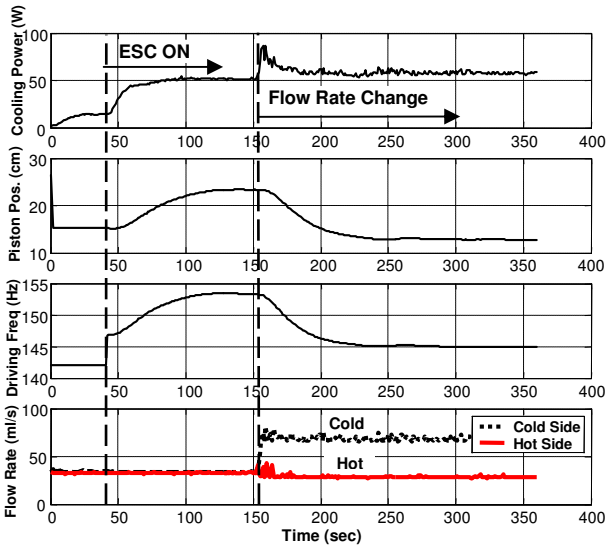

Fig. 5: ESC tuning with varying cold-side flow rate

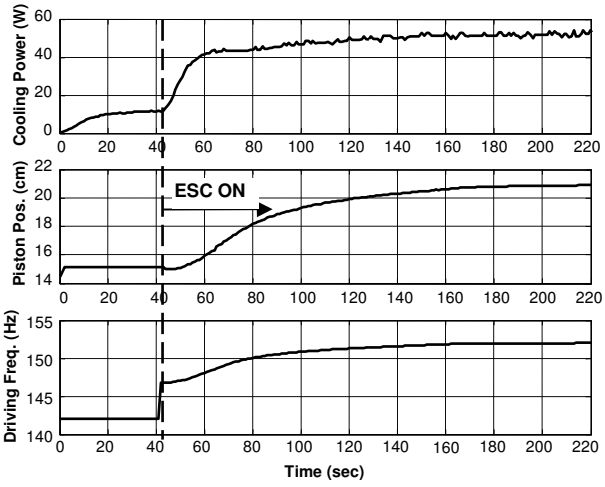

Fig. 6: Test *A* results ($K_{px} = 4$, $K_{dx} = 0$, $K_{pf} = 6$, $K_{df} = 0$)

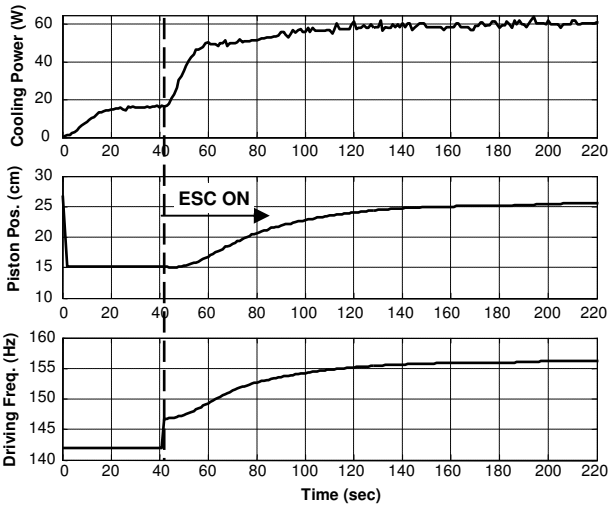

Fig. 7: Test *B* results ($K_{px} = 4$, $K_{dx} = 2$, $K_{pf} = 6$, $K_{df} = 3$)

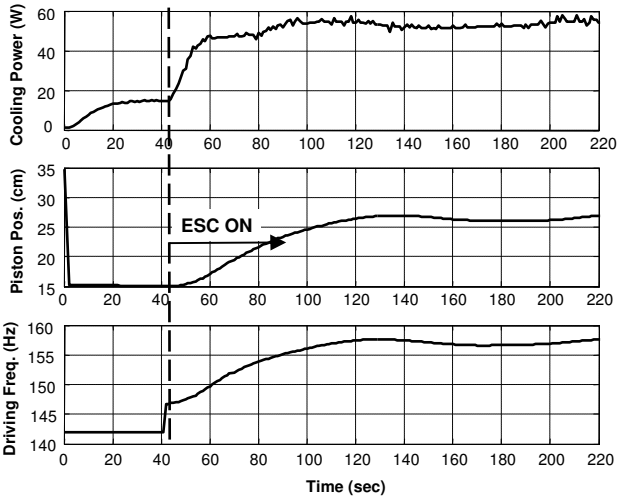

Fig. 8: Test *C* results ($K_{px} = 4$, $K_{dx} = 4$, $K_{pf} = 6$, $K_{df} = 6$)

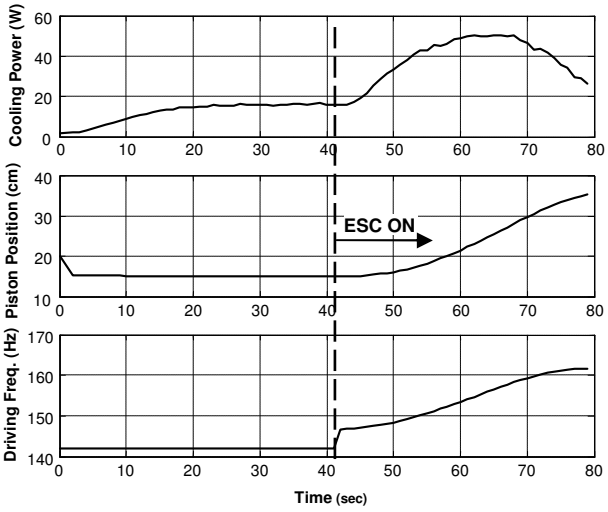

Fig. 9: Test *D* results ($K_{px} = 4$, $K_{dx} = 20$, $K_{pf} = 6$, $K_{df} = 20$)